

https://dspace.org/

The development of a tough high chronmium ferritic stainless steel

Hermanus, Mavis Ann

2015-01-27
http://hdl.handle.net/10539/16775

Downloaded from a DSpace repository. https://dspace.org/

EDS analysis also confirmed the presence of σ in the LNNI alloy. Unfortunately detailed analysis of the σ at the annealed grain boundaries of the V4 alloys could not be provided as these were too fine. The evidence did, however, indicate that they probably had a chromium content of 42 to 43%.

4.7 TRANSMISSION ELECTRON MICROSCOPY

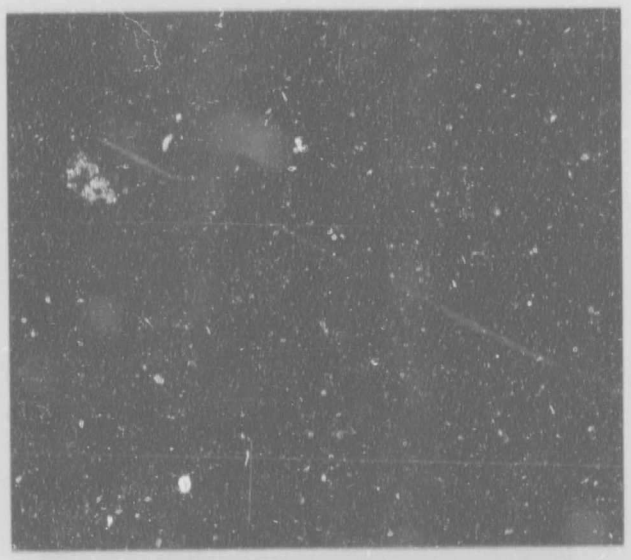
Although the alloys selected contained little σ, one (V4/0) was still embrittled. The causes of embrittlement in this alloy were investigated and the microstructure of the remaining two (V2/1/2 and V4/0,1) were carefully examined for features which could hopefully be uniquely associated with ductile behaviour.

Because the samples were coarse grained, the thin foils which provide limited areas showed few grain boundaries.

4.7.1 Alloy V4/0

Nearly continuous, thin grain boundary precipitation was observed in the brittle V4/0 alloy (Figure 4.35a). In some areas more substantial precipitation had developed (Figure 4.35b). These precipitates were identified (using selected area, SA, diffraction) as M_3C_6 carbides. Centred dark field images of these carbides, their diffraction pattern and its interpretation are given in Figures 3.36 (a, b, c and d). In the diffraction pattern two orientations of the [012] carbide zone axis are apparent. This can be explained in terms of the twinning or faults which can be seen in the dark field images.

Very few dislocations were observed and the presence of many fine intragranular precipitates was also noted (Figure 4.37). Some of these were located along the length of the dislocations.



(a)

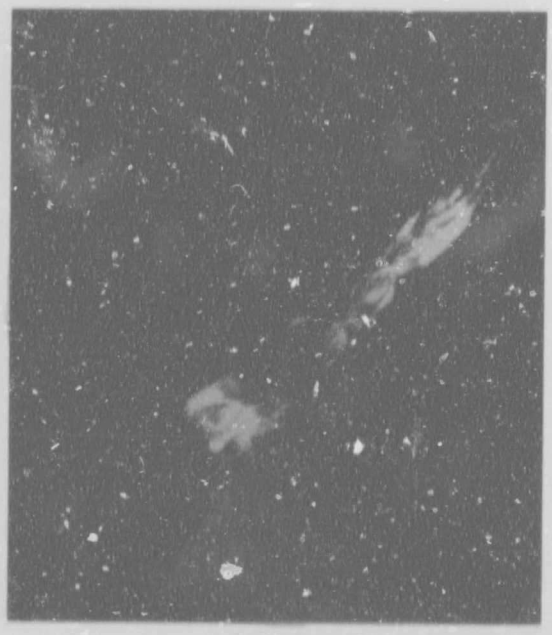


(b)

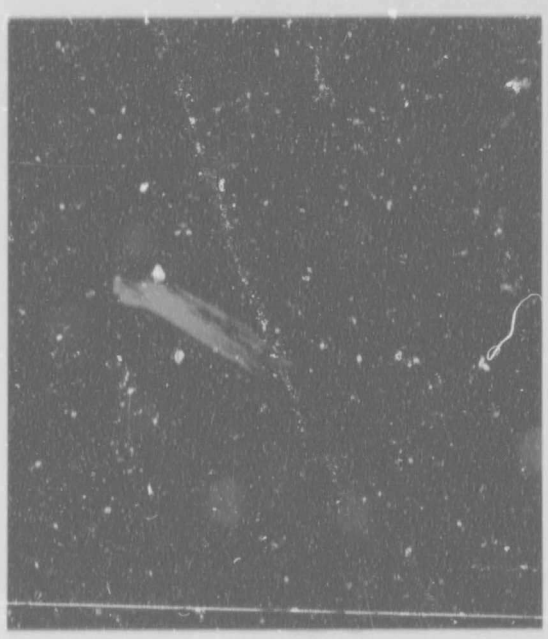
Figure 4.35 Grain boundary precipitation in the brittle V4/0 alloy.

a) Thin grain boundary film.

b) Relatively thick grain boundary precipitation.

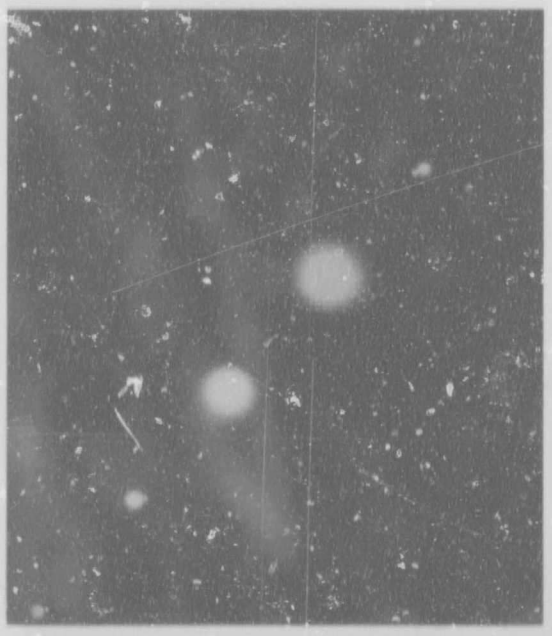


(a)

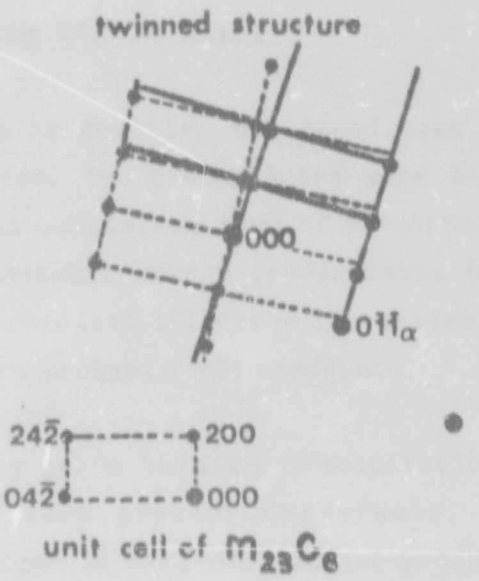


(b)

Figure 4.36 The identification of $M_{23}C_6$ carbides. (a and b) Dark field images of the carbides



(c)



(d)

Figure 4.36 continued

c) Diffraction pattern

d) Interpretation of carbide diffraction pattern.



0,25µm

Figure 4.37 Fine intragranular precipitates in alloy V4/0.

4.7.2 The REM-containing V4/0,1 alloy

This alloy, which is ductile, contained some precipitates along the grain boundaries. The precipitates were largely discrete and many boundary areas completely free of precipitation were observed (Figure 4.38). Occasional coarse precipitates (unidentified) which were totally spheroidised (Figure 4.39) unlike the carbides also occurred. These are probably REM compounds.

In the areas where grain boundary precipitation remained, few or no dislocations were present Conversely, dense tangles of dislocations arranged in well-defined sub-grain boundaries (Figure 4.40) were located in the precipitate-free areas.

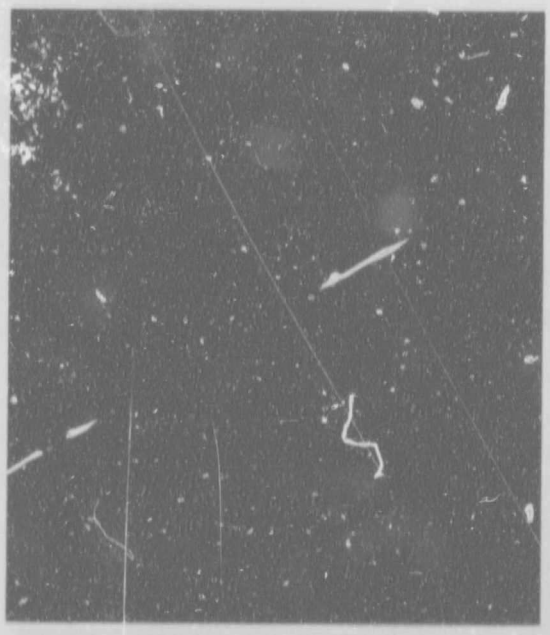


Figure 4.38 Residual grain boundary precipitation in alloy V4/0,1, ductile.



Figure 4.39 Spheroidal precipitate in the V4/0,1 alloy. Note that the grain boundary on either side of the precipitate is 'clean'.



0,5µm

Figure 4.40 Dislocations arranged in sub-grain boundaries in the ductile alloy V4/0,1.

4.7.3 Alloy V2/1/2

In the ductile alloy which does not contain REMs (V2/1/2) very few precipitates were observed. The grain boundaries in this alloy appear very clean (Figure 4.41). Many dislocations were present (Figure 4.42) and occasionally these formed sub-grain boundaries (Figure 4.43).

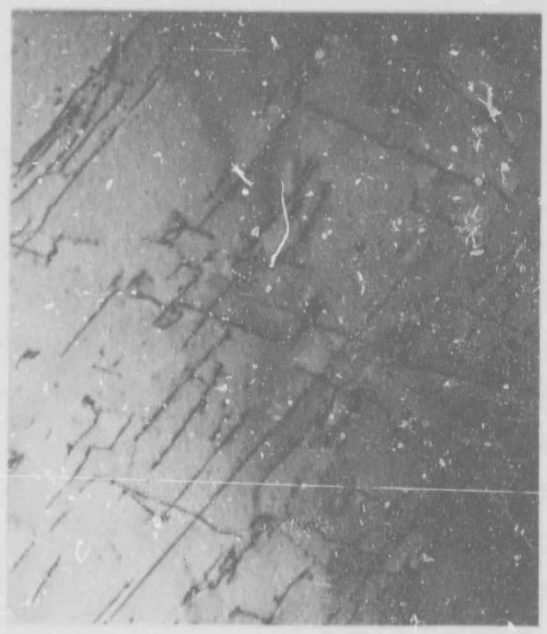
4.7.4 Summary

Brittle behaviour was found to be associated with intragranular and relatively thick grain boundary precipitation. The density of dislocations (high in the ductile alloys and low in the brittle alloy) is probably related to the thickness and continuity of the precipitates at the grain boundary (see section 5.3.3) whereas their mobility is likely to be influenced by the amount of intergranular precipitates. A fine, dense distribution of this would hinder dislocation motion and possibly pin them.



0,5µm

Figure 4.41 Grain boundary free of precipitates in alloy V2/1/2.



1µm

Figure 4.42 Dislocations in alloy V2/1/2.



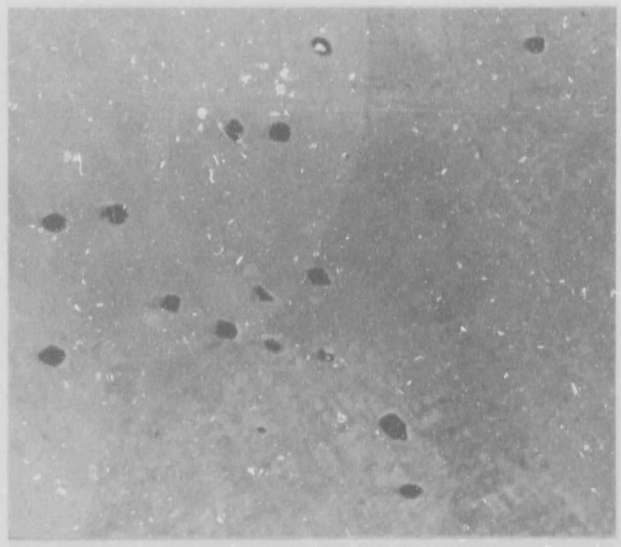
0,5µm

Figure 4.43 Sub-grain boundary in alloy V2/1/2.

4.8 ELECTRON MICROPROBE ANALYSIS

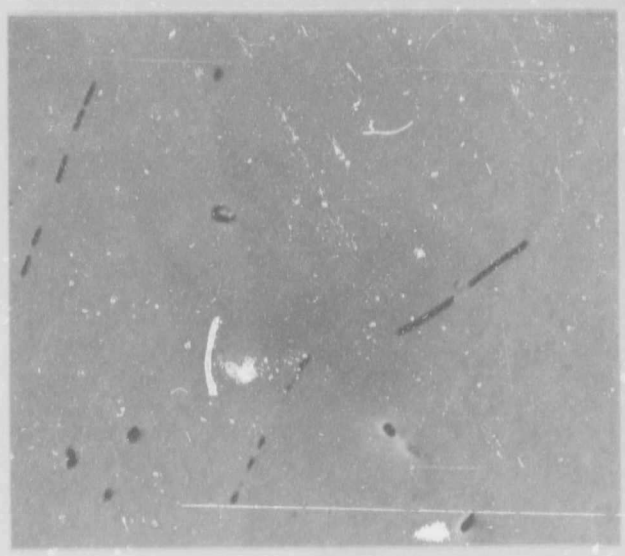
Qualitative electron microprobe analysis was used to identify the elements present in the inclusions in the Fe-40Cr alloys. It also proved possible to indicate the relative concentration of elements such as oxygen. The results of the probe analyses are given in Figures 4.44 to 4.48 below.

The blocky (4.35) and needle-like inclusions (4.36) contained iron, chromium and oxygen. The oxygen content was lower in the latter morphology. In alloy V4/0, cored inclusions were observed (Figure 4.37). The outer rims of these particles contained larger quantities of oxygen than the cores. Sigma (iron and chromium only) was present as long strings of light grey inclusions (Figure 4.38). Numerous intragranular and grain boundary oxides of iron, chromium and REM were observed in the alloy V2/3 which contained excess REMs (0,6%).



5µm

Figure 4.44 (Iron and chromium) oxide inclusions in the V1/1 alloy.



20µm

Figure 4.45 (Iron and chromium) oxide inclusions in the V1/1 alloy. These needle-like oxides contain less oxygen than the blocky oxides.



Figure 4.46 Cored oxide inclusions in the V4/0 alloy. The cores of the oxides contain less oxygen than the rims.

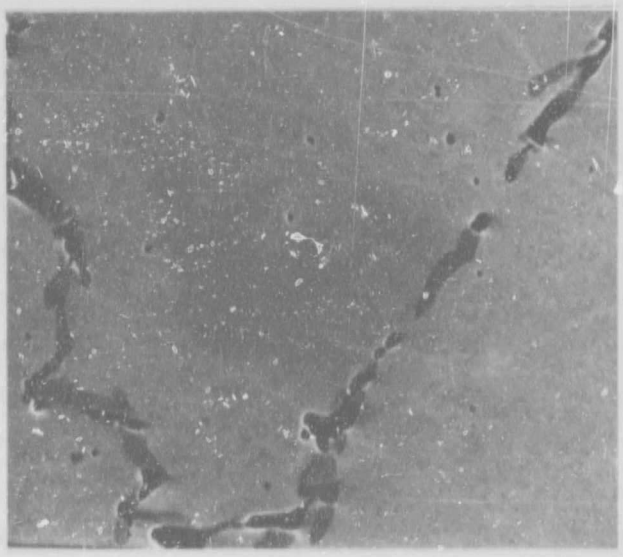


Figure 4.47 The light grey inclusions are σ precipitates (containing iron and chromium). The dark inclusions (aistinguishable from the holes in the stringers) are (iron and chromium) oxides. (Alloy V4/0.)

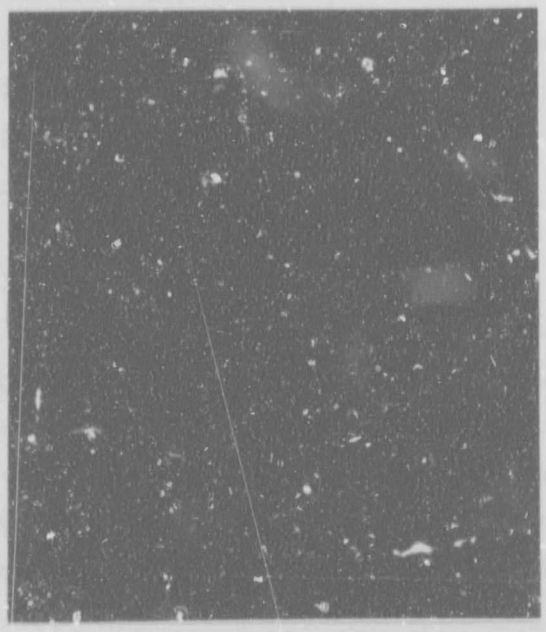


Figure 4.48 All inclusions are mixed oxides: (Fe, Cr, REM)$_x$O$_y$. (Alloy V2/3.)

4.9 IMAGE ANALYSIS

It has been shown that small additions of rare earth metals influence the number, size and shape of inclusions. Different annealing times and temperatures and interstitial element contents have also been shown to affect the characteristics of the inclusions. In a general way these observations have been linked to the toughness of the Fe-40Cr alloys. For example heavy grain boundary precipitation and high interstitial levels have been associated with brittle behaviour.

The image analysis study was an attempt to quantify the data related to the inclusions and to determine whether this data was related to the alloy behaviour in a consistent way.

Transverse sections of six samples were used in this study. The samples were:

(i) the V1 alloy (0% REM) in two conditions: after annealing

at 950°C and 1100°C:

(ii) the V2/1/2 and V4/0 alloys which do not contain REM and of which V2/1/2 was ductile and V4/0 was brittle: and

(iii) the V4/0,1 alloy (containing 0,1% REM) in two conditions: ductile and brittle.

The surfaces of the specimens were polished and viewed in the unetched condition. An automatic sampling facility was used to sample 800 fields of view in each. The inclusions were divided into two classes: needle-like and rounded. For each class four parameters were measured: count, area%, area and the circular shape factor (FORM PE). The sample parameters are now described here in detail to assist in the subsequent consideration of the results.

(i) The 'count' parameter

This parameter counts the number of objects per field. It is effectively a density measure. The spread of the values also gives an indication of the homogeneity of the distribution of inclusions in the samples.The results from each sample are plotted on a histogram which has frequency versus count axes. The mean value is automatically calculated. For a given level of interstitials the mean value gives a useful indication of the extent of precipitation.

(ii) The 'area' parameter

The area of each individual particle in a particular sample is calculated by the area parameter. The axes of the histogram on which the results are plotted are frequency versus particle area. The mean area calculated indicates the average size of the particles in each alloy.

(iii) The 'area %' parameter

To obtain this value, the sum of the areas of each detected inclusion detected is measured and expressed as a percentage of the total area analysed. The results are plotted on a histogram and the mean is automatically calculated. This mean value gives an indication of the

'dirtiness' of each alloy since it is related to the volume percentage of inclusions.

(iv) The 'FORM PE'

The circular shape factor of the particle is defined by the following mathematical expression:

$$\text{FORM PE} = \frac{4 \times \pi \times \text{AREA}}{\text{PERIMETER}}$$

For values equal to unity, the shape factor indicates that particles analysed are perfectly round or square. The closer the values to zero the more elongated and narrow the particles are.

4.9.1 The effect of different annealing temperatures

The results of image analysis on the alloy V1, heat treated at 950 and 1100°C are summarised below.

The annealing treatment at 950°C produced more inclusions than that at 1100°C (a total of 731 inclusions as opposed to 695). Although both classes of inclusions (needle-like and round/blocky) follow this trend it is not significant since standard deviations of the mean number of objects per field were so large that they may overlap.

The count distribution of each class of inclusion was similar in both alloys. 75% of the fields contained between 1 and 5 of the blocky inclusions whereas more than 70% of the fields contained no needle-like inclusions. These results confirmed the observation that the inclusions tend to be unevenly distributed.

For both heat treatments, the blocky inclusions ranged from 0,5 to 19μm^2 in area and most gave areas less than 7μm^2. The areas of the needle-like inclusions clustered around an area of 5μm^2 and none were larger than 9μm^2. Typical area distributions are shown in Figures 4.49 and 4.50.

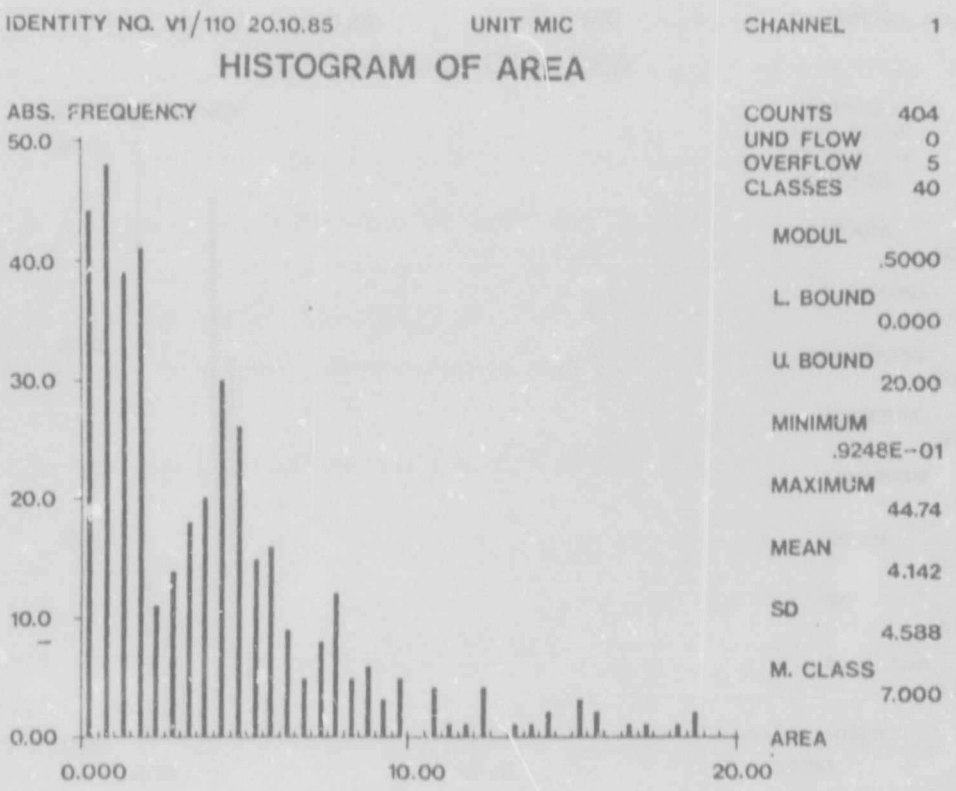


Figure 4.49 Area distrbution of round/blocky precipitates

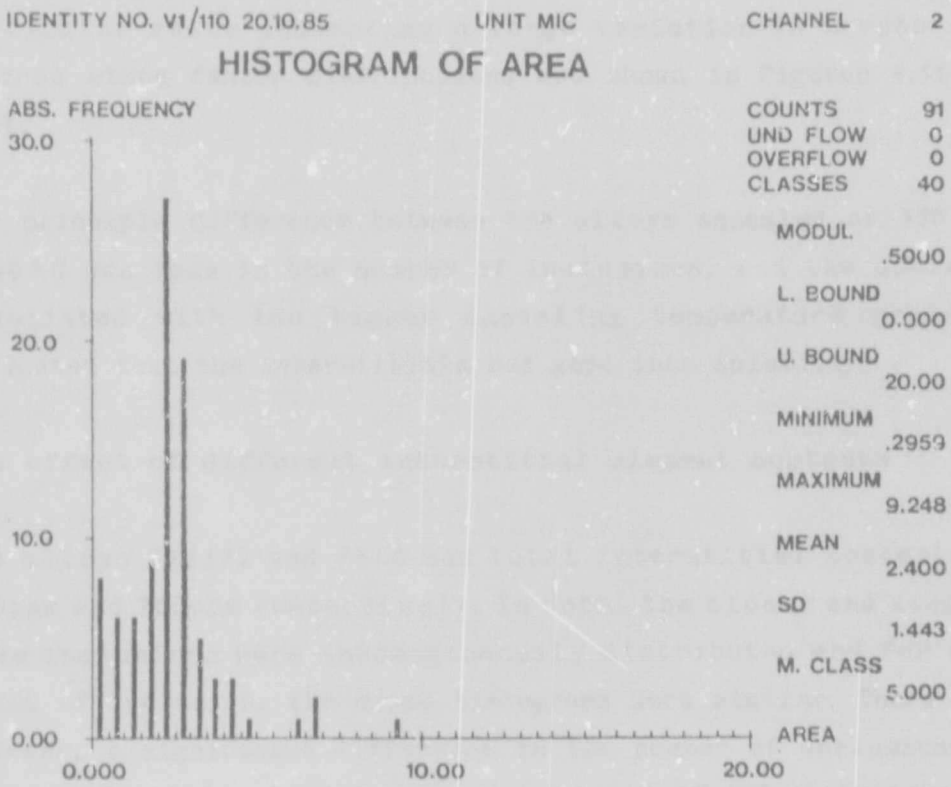


Figure 4.50 Area distribution of needle-like precipitates.

The area % histograms were similar in shape to the area histograms. The inclusions in the alloy annealed at 950°C covered a mean area of 0,17% while the mean area for the inclusions after the 1100°C anneal was 0,16%.

The shape factor distribution of the blocky precipitates was skewed towards unity (perfectly square or round particles) as expected. The needle-like precipitates did not group around any particular value indicating a large variation in morphology. Typical shape factor distributions are shown in Figures 4.51 and 4.52.

The principle difference between the alloys annealed at 950 and 1100°C was thus in the number of inclusions, and the decrease associated with the higher annealing temperature probably indicated that the interstitials had gone into solution.

4.9.2 The effect of different interstitial element contents

The alloys V2/1/2 and V4/0 had total interstitial contents of 460ppm and 760ppm respectively. In both, the blocky and needle-like inclusions were inhomogeneously distributed and for each class of inclusion, the count histograms were similar. There was, however, a significant difference in the number of inclusions in each sample. Alloy V2/1/2 contained a total of 450 inclusions for the 800 fields analysed whereas the corresponding value for the V4/0 alloy was 985. The number of needle-like inclusions was similar to the number of blocky ones in both.

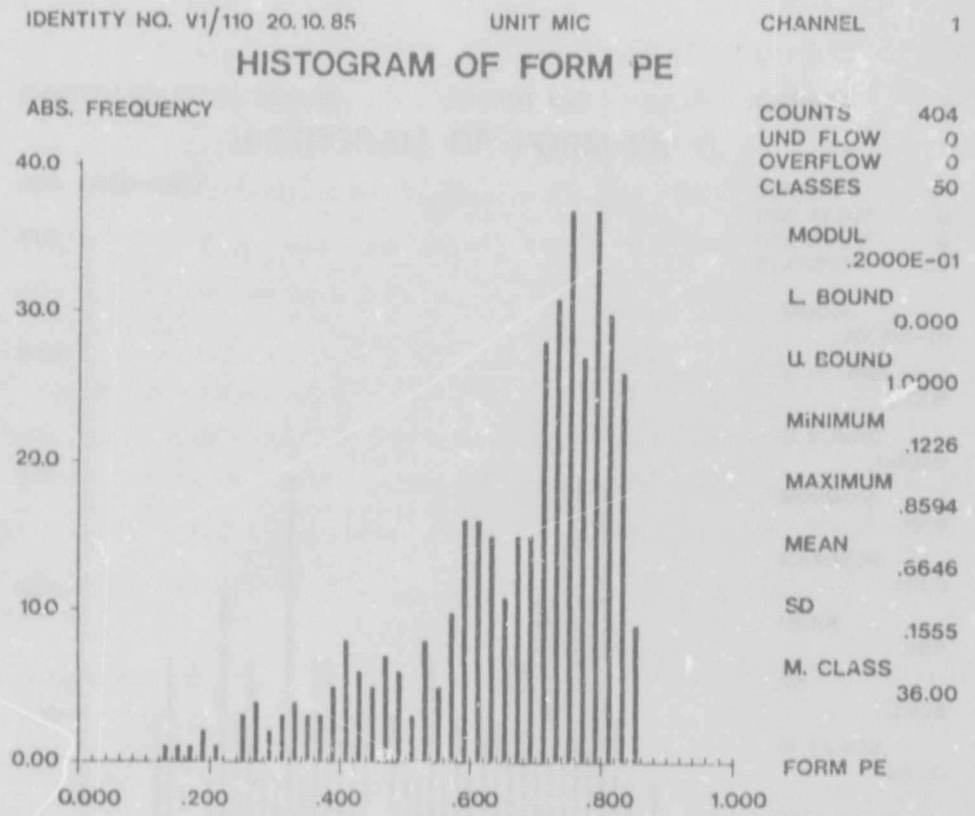


Figure 4.51 Typical shape factor distribution of blocky/round precipitates. The histogram is skewed towards unity (perfect cicularity).

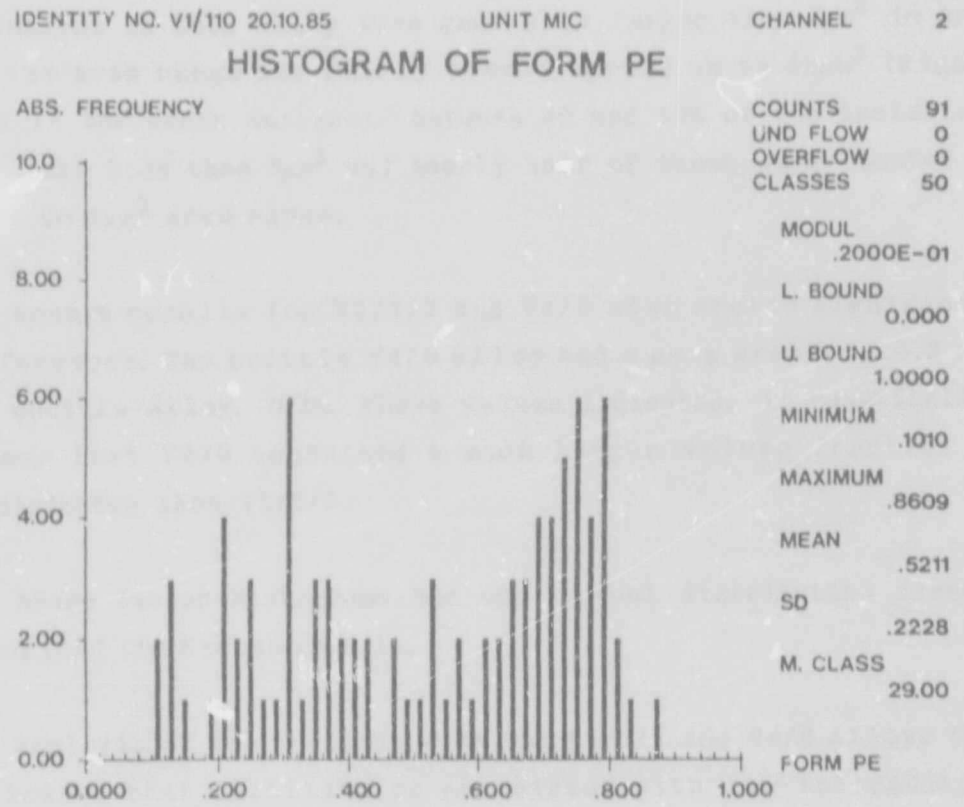


Figure 4.52 Typical shape factor distribution of needle-like inclusions. The wide spread indicates irregularity in shape.

The areas of the blocky inclusions were spread over a wide range (0 - 20μm^2) and that of the needle-like inclusions over a narrow range (0 - 5μm^2). In this instance, the results for the V2/1/2 and V4/0 alloys were similar to those described in Section 4.9.1. However, the distribution of the areas of the blocky inclusions in the ductile alloy (V2/1/2) was significantly different from that of V4/0 (and the other two alloys already analysed). The inclusions in this alloy were generally larger than 1μm^2 in area and the area range was fairly evenly spread up to 20μm^2 (Figure 4.53) In the other analyses, between 60 and 90% of the inclusions had areas less than 5μm^2 and nearly half of these were located in the 0 to 1μm^2 area range.

The area % results for V2/1/2 and V4/0 also showed significant differences. The brittle V4/0 alloy had a mean area % of 0,8 and the ductile alloy, 0,2%. These values indicated, in quantitative terms, that V4/0 contained a much larger volume fraction of precipitates than V2/1/2.

The shape factor histograms had the typical distribution already described (in Section 4.9.1).

The analysis of the inclusions in the V2/1/2 and V4/0 alloys thus indicated that ductility is associated with low interstitial contents, fewer inclusions, and inclusions of a larger size.

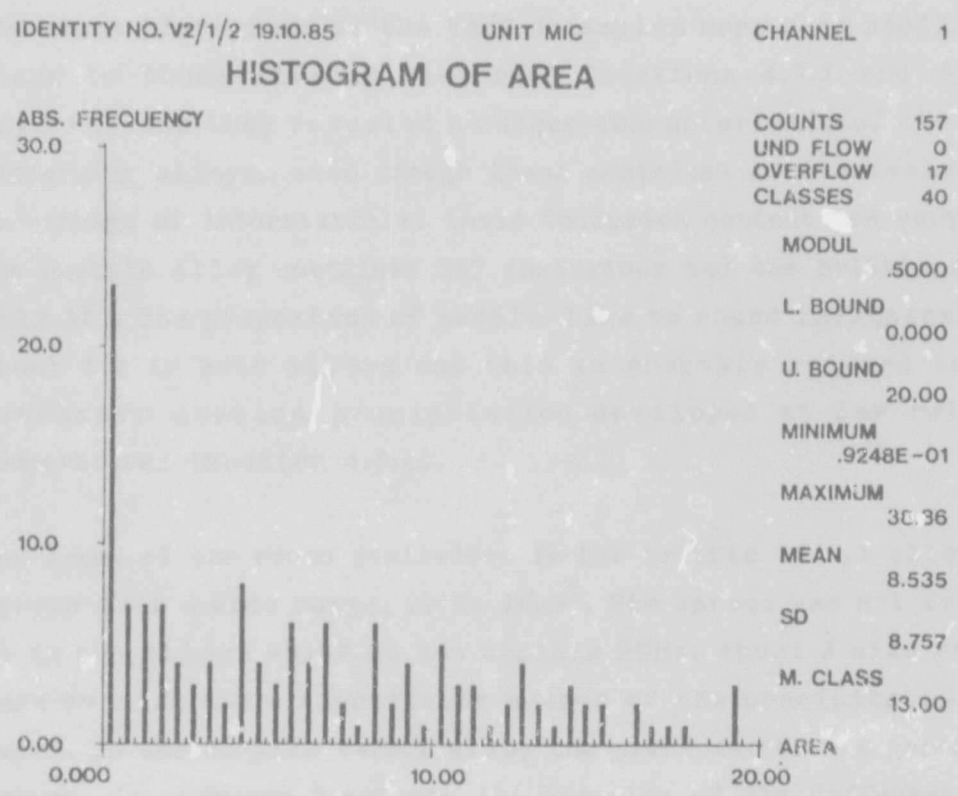


Figure 4.53 V2/1/2 - ductile alloy, area distribution. The inclusions were mainly greater than $1\mu m^2$ in size.

4.9.3 The effect of REM additions

The alloy V4/0,1 which contained 0,10% REM, in the ductile and brittle condition, was compared to V2/1/2. This alloy had a higher interstitial content than V2/1/2; 540ppm as opposed to 460ppm, and due to the presence of REMs, had rounded rather than blocky precipitates.

The count histograms of the V4/0,1 samples were were similar in shape to those already described (Sections 4.9.1 and 4.9.2). Nevertheless they revealed a unique characteristic of the REM-containing alloys; even though these contained a relatively high percentage of interstitials, their inclusion content was very low. The ductile alloy contained 287 inclusions and the brittle alloy only 381. The proportion of needle-like to round inclusions was about 1:1 in both alloys and this is probably related to the extensive carbide precipitation developed at low rolling temperatures (Section 4.5.4).

The areas of the round inclusions in the brittle V4/0,1 alloy was spread over a wide range, up to 20μm^2. The spread was not as even as in the alloys which do not contain REMs. About 3 size ranges were evident and a significant number of the precipitates were small. In the ductile V4/0,1 alloy the precipitates are generally larger, 16 exceeded 20μm^2 and the grouping of the different size ranges was accentuated (Figure 4.54). This should be compared with the smooth variation in the other alloys (cf Figure 4.49). However, this alloy still had a greater percentage of smaller-sized precipitates (<3μm^2) than V2/1/2 which had a higher upper shelf impact energy. In both V4/0,1 alloys, most needle-like inclusions were larger than 1μm^2 in size. In contrast, those in the V2/1/2 alloy were mostly smaller than 1μm^2.

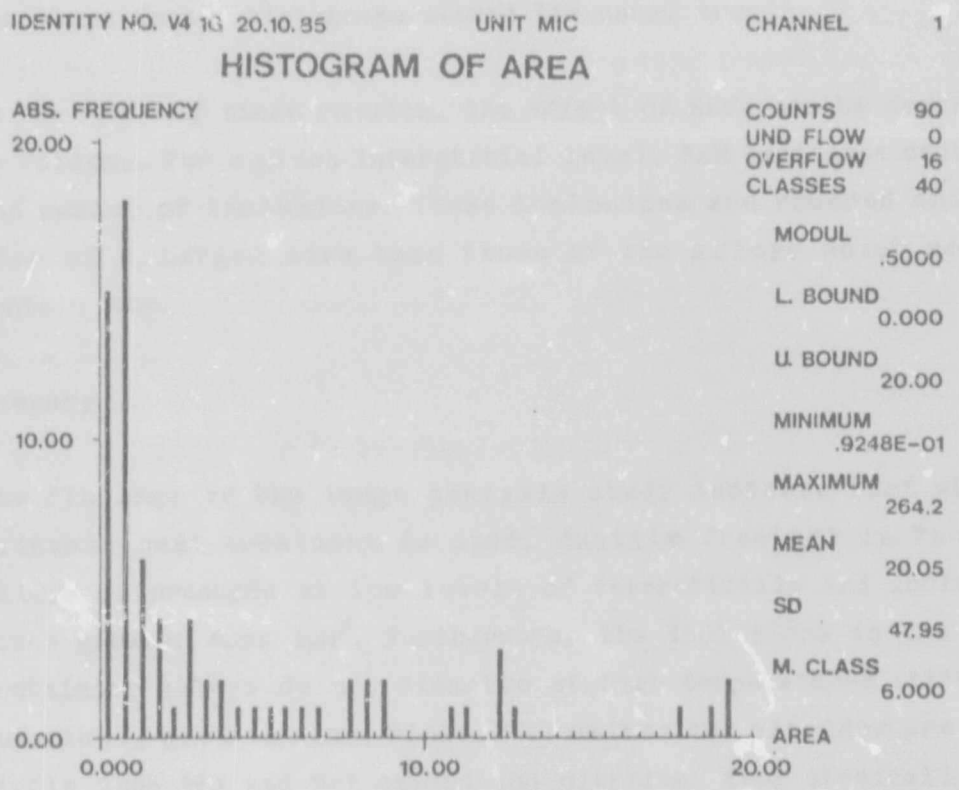


Figure 4.54 Area distribution of a ductile REM-containing alloy. The REM addition separated the inclusions into definite size groupings.

The percentage area occupied by the inclusions in the V4/0,1 alloys was 0,4 and 0,35% for the ductile and brittle conditions respectively. The ductile alloy thus had fewer, but larger precipitates. Alloy V2/1/2, the most ductile of the three alloys examined had an even smaller percentage area (only 0,2%) ascribed to precipitation.

The shape factor histograms showed the usual trends.

On the basis of these results, the effect of REMs can be described as follows. For a given interstitial level, REM additions decrease the number of inclusions. These inclusions are rounded and are also of a larger size than those of the alloys which do not contain REM.

4.9.4 Summary

The findings of the image analysis study indicate that when a suitable heat treatment is used, ductile fracture in Fe-40Cr alloys is produced at low levels of interstitials and inclusion sizes greater than $1\mu m^2$. Furthermore, the inclusions in the REM-containing alloys do not dissolve at high temperatures (1150°C), but simply grow in size. Since, REM oxides and nitrides are more stable than (Fe and Cr) oxides and nitrides, they chemically fix oxygen and nitrogen, and hence decrease the susceptibilty of the alloys to high temperature embrittlement. Finally REM additions spheroidise inclusions. For a given interstitial level, this shape of inclusion appears to promote ductile behaviour.

5 DISCUSSION

5.1. MECHANICAL TEST RESULTS

5.1.1 Comparison between the impact energies obtained in the current study and those quoted in the literature.

Compared with the modest ductile - to - brittle - transition - temperatures (DBTTs) obtained in this study (-15°C at best) the results quoted in the literature seem spectacular. DBTTs of -100, -75 and - 40°C are routinely quoted for alloys containing 18 to 30% chromium[2,8,38,42]. The Charpy specimens used in these reported studies were however only 1,5 to 4mm thick. Table 5.1 lists the specimen thicknesses and the corresponding transition temperatures.

Table 5.1 DBTTs for Charpy impact samples of various thicknesses.

DBTT (°C)	Specimen thickness (mm)	References
-100	1,5	2
-75	1,5 and 2,5	8,42
-40	2,5 and 4	8,38

The practice of using sub-size specimens means that comparison of the results of the different studies is impossible. The Charpy test specifications state that a general correlation between energy values obtained with samples of different sizes is not feasible. Moreover, a study[78] specifically designed to examine specimen size effects showed that the transition temperature in several steels increased dramatically (from -50 to 50°C) with increasing Charpy bar thickness (from 1,25mm to 10mm). Similarly Onashi et al[38] found that increases in the specimen thickness of a 26Cr-Mo alloy from 4mm to the standard 10mm specimen size raised the DBTT by 20 to 30°C. This upward shift of the transition

Author Hermanus Mavis Ann
Name of thesis The development of a tough high chronmium ferritic stainless steel. 1986

PUBLISHER:

University of the Witwatersrand, Johannesburg
©2013

LEGAL NOTICES:

Copyright Notice: All materials on the University of the Witwatersrand, Johannesburg Library website are protected by South African copyright law and may not be distributed, transmitted, displayed, or otherwise published in any format, without the prior written permission of the copyright owner.

Disclaimer and Terms of Use: Provided that you maintain all copyright and other notices contained therein, you may download material (one machine readable copy and one print copy per page) for your personal and/or educational non-commercial use only.

The University of the Witwatersrand, Johannesburg, is not responsible for any errors or omissions and excludes any and all liability for any errors in or omissions from the information on the Library website.